A Bottom-Following Preview Controller for Autonomous Underwater Vehicles

Carlos Silvestre, Rita Cunha, Nuno Paulino, and António Pascoal

***Abstract*—This paper describes a solution to the problem of bottom-following for autonomous underwater vehicles (AUVs) that relies on the evaluation of the terrain characteristics ahead of the vehicle using echo sounders. The methodology used poses the problem as a discrete time path following control problem where a conveniently defined error state space model of the plant is augmented with bathymetric (i.e., depth) preview data. A piecewise affine parameter-dependent model representation is adopted that describes the AUV linearized error dynamics for a predefined set of operating regions. For each region, a state feedback H_2 control problem for affine parameter-dependent systems is posed and solved using linear matrix inequalities (LMIs). The resulting nonlinear controller is implemented as a gain-scheduled controller using the D-methodology. Simulation results obtained with a nonlinear dynamic model of the INFANTE AUV in the vertical plane are presented and discussed.**

***Index Terms*—Discrete time systems, linear parameter varying systems, preview control, tracking, transient response, underwater vehicles.**

I. Introduction

THIS paper describes a solution to the problem of bottom-following controller design for autonomous underwater vehicles (AUVs) that takes explicitly into account the bathymetric characteristics ahead of the vehicle measured by two echo sounders. The methodology adopted falls within the scope of preview control theory. The proposed solution is evaluated in simulation with a model of the prototype INFANTE AUV (see Fig. 1), built and operated by the Instituto Superior Técnico of Lisbon, Portugal.

Preview control algorithms have been widely used to improve the closed loop performance that can be obtained with limited bandwidth feedback compensators when future information about the environment, as reflected in information about future commands and disturbances, is available. A series of papers on the application of Linear Quadratic preview control theory to the design of vehicle active suspensions can be found in the literature. Special emphasis should be given to the pioneering work of Tomizuka [1], where an optimal preview control problem is formulated and solved and the impact of different preview lengths on the overall suspension system performance is discussed. An alternative method is presented in Prokop and Sharp [2] that consists of incorporating the disturbance or reference dynamics into the design model and then solving the resulting linear quadratic control problem. More recently, Takaba [3] addressed the problem of robust LQ/H_∞ servomechanism design with preview action for polytopic uncertain systems using Linear Matrix Inequalities.

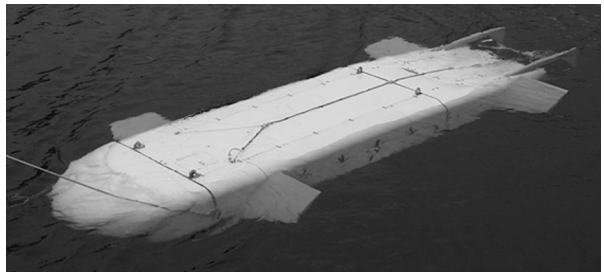

Fig. 1. INFANTE vehicle.

For linear control systems design, the present paper exploits the use of a discrete time state feedback H_2 preview controller synthesis algorithm. In the approach pursued here, the results presented in [3]–[6] are used to develop a linear matrix inequality (LMI)-based H_2 preview controller synthesis algorithm for affine parameter-dependent systems. For large preview intervals, the technique proposed in the paper leads to LMI optimization problems involving a large number of variables. To overcome this limitation, an alternative algorithm for computing the required feedforward gain matrix is presented that exploits the particular structure of the augmented preview system.

In the paper, linear state feedback preview controllers are synthesized for a finite number of piecewise affine parameter-dependent discrete time plant models. Each of these models consists of the discrete equivalent of the generalized error linearization for each of the AUV operating regions determined by a well-defined box in the parameter space (defined by the vehicle's total speed and angle of attack). The error space adopted is in line with the solutions presented in [7]–[9] and includes an important directionality factor that takes into account the current vehicle orientation in the definition of the linear velocity error. The authors have applied a similar technique to a rotorcraft terrain-following problem, the details of which can be found in [10].

The final implementation of the resulting nonlinear gain scheduled controller uses the D-methodology described in

Manuscript received July 21, 2007; revised May 30, 2007. Manuscript received in final form February 12, 2008. First published May 30, 2008; current version published February 25, 2009. Recommended by Associate Editor C. Knospe. This work was supported in part by Fundação para a Ciência e a Tecnologia (ISR/IST pluriannual funding) through the POS_Conhecimento Program that includes FEDER funds, Project GREX/CE- CIST (Contract 035223), Project MAYA-Sub of the AdI (PT), and the FREESUBNET RTN of the CEC.

C. Silvestre and A. Pascoal are with the Department of Electrical Engineering and the Institute for Systems and Robotics, Instituto Superior Técnico, 1049-001 Lisbon, Portugal (e-mail: cjs@isr.ist.utl.pt; antonio@isr.ist.utl.pt).

R. Cunha is with the Institute for Systems and Robotics, Instituto Superior Técnico, 1049-001 Lisbon, Portugal (e-mail: rita@isr.ist.utl.pt).

N. Paulino is with the European Space Agency, ESTEC, 2200 AG, Noordwijk ZH, The Netherlands (e-mail: Nuno.Paulino@esa.int).

Digital Object Identifier 10.1109/TCST.2008.922560

[11], which guarantees a fundamental linearization property and eliminates the need to feedforward the values of the state variables and inputs at trimming. A key question underlying the design of sensor based bottom-following control systems is the computation of the bottom elevation data from sonar measurements. In this paper, the technique adopted exploits the sensor geometry to efficiently build the seabed profile ahead of the vehicle.

The paper is organized as follows. Section II introduces a nonlinear model for the vertical plane dynamics of the INFANTE AUV. Section III, in which the problem of bottom-following is formulated, introduces briefly the path-dependent error space used to describe the vehicle dynamics. Section IV states the preview control problem. Section V describes the methodology adopted for H_2 linear controller design whereby an LMI synthesis technique is applied to affine parameter-dependent systems. Section VI presents the reconstruction technique used to build the reference path from sonar profiler measurements. Section VII focuses on the implementation of the nonlinear bottom-following controller for the INFANTE AUV. Finally, simulation results obtained with a vertical plane nonlinear dynamic model of the vehicle are presented in Section VIII.

II. Vehicle Dynamics

Here, we describe the dynamic model of the INFANTE AUV in the vertical plane. See [12] and [13] for details. The vehicle is 4.5 m long, 1.1 m wide, and 0.6 m high. It is equipped with two main thrusters (propellers and nozzles) for cruising and fully moving surfaces (rudders, bow planes, and stern planes) for vehicle steering and diving in the horizontal and vertical planes, respectively. The notation used and the structure of the vehicle model are standard [12], [14]. The variables u and w denote surge and heave speeds, while θ, q, x, and z denote pitch, pitch rate, x-inertial position, and depth, respectively. The symbols δ_b and δ_s represent the bow and stern plane deflections, respectively. With this notation and neglecting the stable roll mode, the dynamics of the AUV in the vertical plane can be written in compact form as

$$\begin{aligned}
m\dot{u} &= X_{uu}u^2 + X_{ww}w^2 + X_{qq}q^2 + u^2X_{\delta_b\delta_b}\delta_b^2 \\
&\quad + u^2X_{\delta_s\delta_s}\delta_s^2 + X_{\dot{u}}\dot{u} + T && (1)\\
\dot{x} &= u\cos(\theta) + w\sin(\theta) && (2)\\
m(\dot{w} - uq) &= (W - B)\cos(\theta) + \frac{\rho}{2}L^2Z_w uw \\
&\quad + \frac{\rho}{2}L^3Z_q uq + \frac{\rho}{2}L^2u^2\left[Z_{\delta_b}\delta_b + Z_{\delta_s}\delta_s\right] \\
&\quad + \frac{\rho}{2}L^3Z_{\dot{w}}\dot{w} + \frac{\rho}{2}L^4Z_{\dot{q}}\dot{q} && (3)\\
\dot{z} &= -u\sin(\theta) + w\cos(\theta), && (4)\\
I_y\dot{q} &= z_{CB}B\sin(\theta) + \frac{\rho}{2}L^3M_w uw + \frac{\rho}{2}L^4M_q uq \\
&\quad + \frac{\rho}{2}L^3u^2[M_{\delta_b}\delta_b + M_{\delta_s}\delta_s] \\
&\quad + \frac{\rho}{2}L^4M_{\dot{w}}\dot{w} + \frac{\rho}{2}L^5M_{\dot{q}}\dot{q} && (5)\\
\dot{\theta} &= q && (6)
\end{aligned}$$

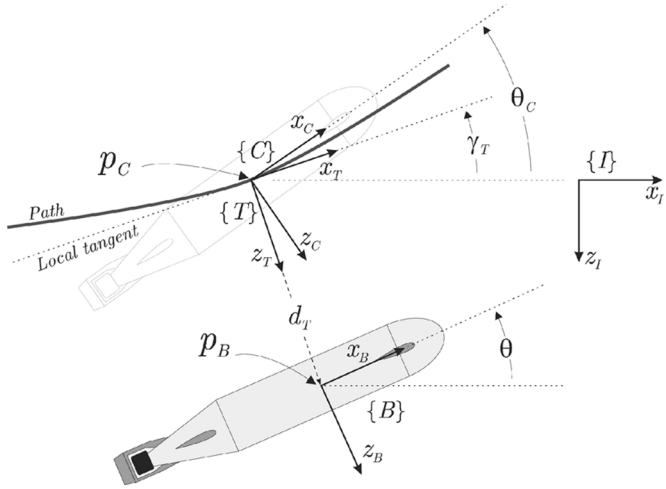

Fig. 2. Coordinate frames: inertial $\{I\}$; body-frame $\{B\}$; Serret–Frenet $\{T\}$; desired body-frame $\{C\}$.

where (1), (3), and (5) describe the surge, heave, and pitch motion, respectively, $X_{(.)}$, $Z_{(.)}$, and $M_{(.)}$ are hydrodynamic derivative terms, and z_{CB} represents the metacentric distance. Equations (2), (4), and (6) capture the vehicle kinematics. See [12] and [13] for numerical values of the hydrodynamic parameters. The variables m, L, W, B, and I_y are the vehicle's mass, length, weight, buoyancy, and moment of inertia about the y axis, respectively and ρ is the density of the water.

III. Error Space

The problem of steering the vehicle along a predefined path, which ultimately allows for definition of a bottom-following controller, can be converted into a regulation problem by expressing the state of the vehicle in a specifically (and conveniently) defined error space. This requires the introduction of two coordinate systems: 1) the Serret–Frenet frame $\{T\}$ with origin at the point on the path closest to the vehicle and coordinate axes corresponding to the tangent and binormal vectors defined at that point and 2) the desired body reference frame $\{C\}$ determined as if the vehicle were following the path with zero error, see Fig. 2. Notice that $\{C\}$ is highly dependent on the vehicle dynamics. However, as will be seen later, $\{C\}$ will never be computed explicitly. A reference for the tangent velocity is also required, with $\mathbf{v}_r = [V_r\ 0]^T$ denoting the desired linear velocity in 2-D, expressed in $\{T\}$.

Given these definitions, and simplifying the error space presented in [7] for the 2-D case, vector $\mathbf{x}_e = [\mathbf{v}_e\ q_e\ d_T\ \theta_e]^T \in \mathbb{R}^5$; $\mathbf{v}_e \in \mathbb{R}^2$ can be introduced with

$$\mathbf{x}_e = \begin{bmatrix} \mathbf{v}_e \\ q_e \\ d_T \\ \theta_e \end{bmatrix} = \begin{bmatrix} \mathbf{v} - \mathrm{R}(\gamma_T - \theta)\mathbf{v}_r \\ q - q_C \\ (x - x_C)\sin(\gamma_T) + (z - z_C)\cos(\gamma_T) \\ \theta - \theta_C \end{bmatrix} \quad (7)$$

where $\mathbf{v} = [u\ w]^T$, vectors $[x\ z]^T$ and $[x_C\ z_C]^T$ are the origins of $\{B\}$ and $\{C\}$, respectively, expressed in $\{I\}$, θ_C is the pitch angle that represents the orientation of $\{C\}$ with respect to $\{I\}$, q_C is the respective time derivative, γ_T is the flight path angle, and $\mathrm{R}(\eta)$ represents the rotation by angle η. Let

$\mathbf{u} = [\delta_b,\ \delta_s,\ T]^T$ be the vector of control inputs. It is straightforward to verify that the vehicle follows the path with tangent velocity $\mathbf{v}_r$ and orientation θ_C if and only if $\mathbf{x}_e = 0$.

Assuming that the reference path is a straight line, $\dot{V}_r = 0$ and $\dot{q}_C = 0$ and the simplified error dynamics can be written as

$$\begin{cases} \dot{\mathbf{v}}_e &= \dot{\mathbf{v}} - \dot{\mathrm{R}}(-\theta)\mathrm{R}(\gamma_T)\mathbf{v}_r - \mathrm{R}(-\theta)\frac{d}{dt}\mathrm{R}(\gamma_T)\mathbf{v}_r \\ \dot{q}_e &= \dot{q} \\ \dot{d}_T &= -u_e \sin(\theta - \gamma_T) + w_e \cos(\theta - \gamma_T) \\ \dot{\theta}_e &= q - \dot{\theta}_C. \end{cases} \tag{8}$$

Notice that, at trimming, $(d/dt)\mathrm{R}(\gamma_T)\mathbf{v}_r = 0$ and $q_C = \dot{\theta}_C = 0$. However, to account for the preview action, these terms are included in the dynamics. Further details on the derivation of the error dynamics can be found in [7]. We also introduce the output vector

$$\mathbf{y}_e = \mathbf{v}_e + \mathrm{R}(\gamma_T - \theta)[0\ d_T]^T \tag{9}$$

that is used for tracking purposes and corresponds to a combination of error vector components expressed in the body coordinate system. By including $\mathbf{v}_e$ and d_T in $\mathbf{y}_e$, both the velocity and position errors are being considered, with the distance vector expressed in the current body frame. Notice that $\mathbf{y}_e$ can be rewritten as $\mathbf{y}_e = \mathbf{v} - R(\gamma_T - \theta)[V_r - d_T]^T$, thus effectively defining a new desired velocity that points towards the path as a function of d_T. In addition, $\mathbf{y}_e$ verifies the following result.

1) Result 1: Consider the AUV vertical plane dynamic model described by (2)–(6) and assume that the vehicle satisfies a trimming condition with the bow plane deflection $\delta_b = 0$. Let $\mathbf{x}_e$ and $\mathbf{y}_e$ be the errors vectors defined with respect to the trimming condition. Then, $\mathbf{x}_e = 0$ if and only if $\mathbf{y}_e = 0$.

Proof: Given (7) and (9), it is obvious that $\mathbf{x}_e = 0$ implies $\mathbf{y}_e = 0$. To show that $\mathbf{y}_e = 0$ is also sufficient for $\mathbf{x}_e = 0$ to hold, we start by noting that, by definition, the vehicle satisfies a trimming condition if $\dot{u} = \dot{w} = \dot{q} = \dot{\theta} = 0$ and $\dot{\mathbf{u}} = 0$. It follows from $\dot{\theta} = 0$ that $q = 0$ and therefore $q_e = 0$. Furthermore, the time derivative of $\mathbf{y}_e = 0$ yields

$$\begin{aligned} \dot{\mathbf{y}}_e = 0 \Leftrightarrow \dot{\mathbf{v}}_e &= \frac{d}{dt}(-R(\gamma_T - \theta)[0\ d_T]^T) \\ &\Leftrightarrow \frac{d}{dt}(\mathbf{v} - R(\gamma_T - \theta)[V_r\ 0]^T) = -R(\gamma_T - \theta)[0\ \dot{d}_T]^T \\ &\Leftrightarrow \dot{d}_T = 0. \end{aligned}$$

From $\dot{d}_T = 0$ and $\mathbf{v}_e = -R(\gamma_T - \theta)[0\ d_T]^T$, it follows that

$$\begin{aligned} u_e \sin(\theta - \gamma_T) = w_e \cos(\theta - \gamma_T) \\ \Leftrightarrow \sin^2(\theta - \gamma_T) d_T = \cos^2(\theta - \gamma_T) d_T \\ \Leftrightarrow d_T = 0 \end{aligned}$$

and therefore $\mathbf{v}_e = 0$. Finally, to show that $\theta_e = 0$, note that, if we consider the additional constraint on the bow plane deflection $\delta_b = 0$, then the vehicle dynamics described by (1), (3), and (5) automatically constrain the pitch angle to verify $\theta = \theta_C$. ■

A. Error Linearization and Discretization

For a given straight line path ($q_C = 0$), constant speed V_r, and flight path angle γ_T, define $\mathbf{u}_C$ as the constant input vector that satisfies (1), (3), and (5) at equilibrium ($\dot{u} = 0$, $\dot{w} = 0$, $\dot{q} = 0$), with $\mathbf{v} = \mathrm{R}(\gamma_T - \theta_C)\mathbf{v}_r$, and $\theta = \theta_C$. Then, the linearization of (8) with output vector $\mathbf{y}_e$ about the equilibrium point $\mathbf{x}_e = 0$, $\mathbf{u} = \mathbf{u}_C$, yields

$$\delta\dot{\mathbf{x}}_e = A_e(\boldsymbol{\zeta})\delta\mathbf{x}_e + B_e(\boldsymbol{\zeta})\delta\mathbf{u} \tag{10}$$

$$\delta\mathbf{y}_e = C_e(\boldsymbol{\zeta})\delta\mathbf{x}_e \tag{11}$$

where $A_e(\boldsymbol{\zeta})$, $B_e(\boldsymbol{\zeta})$, and $C_e(\boldsymbol{\zeta})$ denote the Jacobians evaluated at the equilibrium condition parameterized by $\boldsymbol{\zeta} = [V_r, \gamma_T]^T$.

The discrete time equivalent of the linear continuous time model (10) is obtained using the zeroth-order hold on the inputs technique, with sampling time T. In addition, discrete time integral action (eigenvalues at $z = 1$) is applied to the output so that the discrete time error dynamics can be written as

$$\mathbf{x}_d(k+1) = A(\boldsymbol{\zeta})\mathbf{x}_d(k) + B(\boldsymbol{\zeta})\mathbf{u}(k) \tag{12}$$

where, with an obvious abuse of notation, $\mathbf{x}_d(k) = [\mathbf{x}_e(k)^T, \mathbf{x}_i(k)^T]^T$, $A(\boldsymbol{\zeta}) = \begin{bmatrix} e^{A_e(\boldsymbol{\zeta})T} & 0 \\ C_e(\boldsymbol{\zeta}) & I \end{bmatrix}$, and $B(\boldsymbol{\zeta}) = \begin{bmatrix} \int_0^T e^{A_e(\boldsymbol{\zeta})\tau} d\tau B_e(\boldsymbol{\zeta}) \\ 0 \end{bmatrix}$ for $\boldsymbol{\zeta}$ constant.

IV. Preview Problem Formulation

Better AUV bottom-following performance with limited bandwidth compensators can be achieved by taking into account, in the control law, the seabed characteristics ahead of the AUV obtained from measurements of two echo sounders. The technique used in this paper to develop a tracking controller amounts to augmenting the discrete time error space dynamics with a description of the future evolution of the seabed as measured by the sensors installed on the AUV.

With the objective of including future path disturbances in the discrete time error space dynamics (12), assume that the AUV moves with constant speed along a continuous reference path that results from the concatenation of straight lines. A detailed analysis of the error dynamics (8) suggests the introduction of vector

$$\left[-\left(\mathrm{R}(-\theta)\frac{d}{dt}\mathrm{R}(\gamma_T)\mathbf{v}_r \right)^T,\ 0,\ 0,\ -\dot{\theta}_C \right]^T \tag{13}$$

as the perturbation to be previewed. To this effect, assume that there is a discontinuity in the slope of the reference path, which results from the concatenation of two straight lines and is crossed by the vehicle at time $t = t_0$, as depicted in Fig. 3.

Then, the elements of vector (13) can be rewritten as

$$\begin{aligned} \frac{d}{dt}\mathrm{R}(\gamma_T)\mathbf{v}_r &= \delta(t - t_0)\left(\mathrm{R}(\gamma_T(t_0^+)) - \mathrm{R}(\gamma_T(t_0^-)) \right)\mathbf{v}_r \\ \dot{\theta}_C &= \delta(t - t_0)\left(\theta_C(t_0^+) - \theta_C(t_0^-) \right) \end{aligned}$$

where $\delta(t - t_0)$ is the Dirac's delta function. From (10), the resulting linear error dynamics can be written as

$$\delta\dot{\mathbf{x}}_e = A_e(\boldsymbol{\zeta})\delta\mathbf{x}_e + B_e(\boldsymbol{\zeta})\delta\mathbf{u} + W(\boldsymbol{\zeta})\delta\mathbf{w} \tag{14}$$

with injection matrix

$$W(\boldsymbol{\zeta}) = -\begin{bmatrix} \mathrm{R}(-\theta_C) & \mathbf{0}_{2\times 1} \\ \mathbf{0}_{1\times 2} & 0 \\ \mathbf{0}_{1\times 2} & 1 \end{bmatrix}.$$

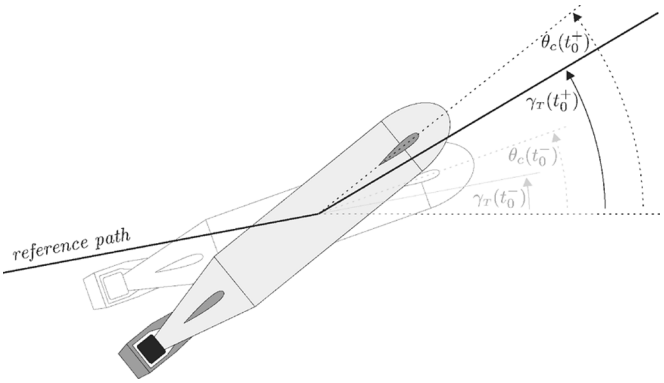

Fig. 3. Reference path—slope discontinuity.

Using this interpretation, the seabed disturbance signal, as seen by the AUV, can be modeled as $\mathbf{s}(t) = \sum_i \mathbf{s}(t_i)\delta(t-t_i)$, where $\mathbf{s}(t_i)$ represents an intensity vector and t_i corresponds to the ith concatenation point crossing time. The corresponding discretization is given by

$$\mathbf{x}_d(k+1) = A(\boldsymbol{\zeta})\mathbf{x}_d(k) + B(\boldsymbol{\zeta})\mathbf{u}(k) + B_1(\boldsymbol{\zeta})\mathbf{s}(k) \quad (15)$$

where $B_1(\boldsymbol{\zeta}) = [(e^{A_e(\boldsymbol{\zeta})T}W(\boldsymbol{\zeta}))^T, 0]^T$ is obtained from the impulse invariant discrete equivalent of the injection matrix $W(\boldsymbol{\zeta})$. It is assumed that the sampling period is sufficiently small to consider the reference path changes synchronized with the sampling time. Once again, with an obvious abuse of notation, $\mathbf{s}(k) \in \mathbb{R}^s$ corresponds to

$$\mathbf{s}(k) = \begin{bmatrix} \left(\mathrm{R}(\gamma_T(t_k^+)) - \mathrm{R}(\gamma_T(t_k^-))\right)\mathbf{v}_r \\ \theta_C(t_k^+) - \theta_C(t_k^-) \end{bmatrix}.$$

Assuming a preview length of p samples, let $\mathbf{x}_s(k) = [\mathbf{s}(k)^T, \mathbf{s}(k+1)^T, \ldots, \mathbf{s}(k+p)^T]^T \in \mathbb{R}^{(s(p+1))\times 1}$ be the vector containing all the preview inputs at instant k. The discrete time dynamics of vector $\mathbf{x}_s(k)$ can be modeled as a FIFO queue, given by

$$\mathbf{x}_s(k+1) = D\mathbf{x}_s(k) + B_s\mathbf{s}(k+p+1) \quad (16)$$

where

$$D = \begin{bmatrix} 0 & I & 0 & \cdots & 0 \\ 0 & 0 & I & \cdots & 0 \\ \vdots & \vdots & \ddots & \ddots & \vdots \\ 0 & 0 & 0 & \ddots & I \\ 0 & 0 & 0 & \cdots & 0 \end{bmatrix}$$

$$B_s = \begin{bmatrix} 0 \\ 0 \\ \vdots \\ I \end{bmatrix}.$$

Combining the dynamic representation of the seabed (16) with(15) yields the augmented system

$$\mathbf{x}(k+1) = \bar{A}\mathbf{x}(k) + \bar{B}_s\mathbf{s}(k) + \bar{B}\mathbf{u}(k) \quad (17)$$

where

$$\mathbf{x}(k) = \begin{bmatrix} \mathbf{x}_d(k) \\ \mathbf{x}_s(k) \end{bmatrix}$$

$$\bar{A} = \begin{bmatrix} A & H \\ 0 & D \end{bmatrix}$$

$$\bar{B}_s = \begin{bmatrix} 0 \\ B_s \end{bmatrix}$$

$$\bar{B} = \begin{bmatrix} B \\ 0 \end{bmatrix}$$

and $H = [B_1, 0, 0, \ldots, 0]$ represents the injection matrix of the preview signals into the error dynamics. Notice that the D matrix is stable and therefore the augmented system (17) preserves the stabilizability and detectability properties of the original plant.

With the technique proposed, the preview information is retrieved at p points selected along the path, equally spaced by the distance $d_p = V_t(k)T$. The scalar $V_t(k)$ corresponds to the norm of the projection of the vehicle's velocity vector $\mathbf{v}$ on the path, computed at instant k, which can be obtained from $V_t = [1\,0]\mathrm{R}(\theta - \gamma_T)\mathbf{v}$. This fact turns out to be of utmost importance, since it allows for a natural redefinition of the controller visibility distance as a function of the vehicle's speed, thus preserving the size of the preview input vector.

V. Discrete Time Controller Design

Here we present a solution to the discrete time state feedback H_2 preview control problem for affine parameter-dependent systems. In the approach pursued in this paper, the results presented in [3]–[6] were used to develop an LMI-based controller synthesis algorithm. Much of the work in this area is well rooted in the theory of LMIs, which are steadily becoming a standard tool for advanced control system design. In fact, LMIs provide a powerful formulation framework as well as a versatile design technique for a wide variety of linear control problems. Since solving LMIs is a convex optimization problem for which numerical solvers are readily available, an LMI based formulation can be seen as a practical solution for many control problems.

A. Theoretical Background

In what follows, the standard setup and nomenclature used in [15] for control problem formulation are adopted, leading to the state-space feedback system represented in Fig. 4. Consider the generalized affine parameter-dependent system $\mathbf{G}(\boldsymbol{\zeta})$ as a function of the varying parameter vector $\boldsymbol{\zeta}$ and assume that $\boldsymbol{\zeta}$ is in a compact set $\Theta \in \mathbb{R}^q$. Suppose that the parameter set Θ can be partitioned into a family of regions that are compact closed subsets Θ_i, $i = 1, \ldots, N$, covering the desired AUV

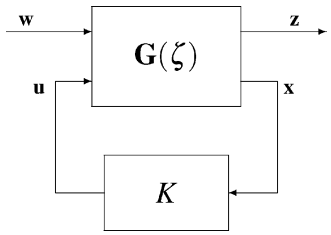

Fig. 4. Feedback interconnection.

flight envelope. In the ith parameter region $\boldsymbol{\zeta} \in \Theta_i$, the dynamic behavior of the closed-loop system admits the realization

$$\begin{cases} \mathbf{x}(k+1) = A(\boldsymbol{\zeta})\mathbf{x}(k) + B_w(\boldsymbol{\zeta})\mathbf{w}(k) + B(\boldsymbol{\zeta})\mathbf{u}(k) \\ \mathbf{z}(k) = C_z(\boldsymbol{\zeta})\mathbf{x}(k) + E(\boldsymbol{\zeta})\mathbf{u}(k), \;\; \mathbf{u}(k) = \mathrm{K}\mathbf{x}(k) \end{cases} \tag{18}$$

where $\mathbf{x}(k)$ is the state vector. The symbol $\mathbf{w}(k)$ denotes the input vector of exogenous signals (including commands, disturbances, and preview signals), $\mathbf{z}(k)$ is the output vector of errors to be reduced during the controller design process, and $\mathbf{u}(k)$ is the vector of actuation signals. Matrices $A(\boldsymbol{\zeta})$, $B_w(\boldsymbol{\zeta})$, $B(\boldsymbol{\zeta})$, $C_z(\boldsymbol{\zeta})$, and $E(\boldsymbol{\zeta})$ are affine functions of the parameter vector $\boldsymbol{\zeta} = [\zeta_1, \ldots, \zeta_q]^T$, e.g., $A(\boldsymbol{\zeta}) = A^{(0)} + \zeta_1 A^{(1)} + \cdots + \zeta_q A^{(q)}$. The generalized affine parameter-dependent system $\mathrm{G}(\boldsymbol{\zeta})$ consists of the plant to be controlled, together with appended weights that shape the exogenous and internal signals and the preview dynamics presented in Section IV.

For a given parameter region $\Delta \equiv \Theta_i$, assume that the elements that constitute the parameter vector $\boldsymbol{\zeta}$ have their values confined to the interval $\zeta_j \in [\underline{\zeta}_j, \overline{\zeta}_j]$, $\overline{\zeta}_j \geq \underline{\zeta}_j$, $j = 1, \ldots, q$, and define Δ_0 as the set of the $m = 2^q$ vertices of the parameter-dependent region

$$\Delta_0 := \{\boldsymbol{\zeta} = [\zeta_1, \ldots, \zeta_q]^T : \zeta_j \in \{\underline{\zeta}_j, \overline{\zeta}_j\},\, j = 1, \ldots, q\}.$$

Then, Δ corresponds to the convex hull of Δ_0, $\Delta = co\{\Delta_0\}$, which is the smallest convex set containing all of the points in Δ_0. The affine parameter-dependent structure provides a powerful set of results when used in conjunction with the following lemma.

1) Result 2: [4] Let $f : \Delta \to \mathbb{R}$ be a convex function where $\Delta = co\{\Delta_0\}$. Then, $f(\boldsymbol{\zeta}) \leq \gamma$, $\forall\, \boldsymbol{\zeta} \in \Delta$, if and only if $f(\boldsymbol{\zeta}) \leq \gamma$, $\forall\, \boldsymbol{\zeta} \in \Delta_0$.

This result allows for the test of quadratic stability and the evaluation of a whole range of performance measures by simply considering a finite number of LMIs, provided that these are convex functions of the parameter vector $\boldsymbol{\zeta}$. In the current case, we are interested in finding a solution to the discrete-time state feedback H_2 synthesis problem. It is well known that the H_2 norm for linear time-invariant (LTI) systems affords several different interpretations, namely those based on the response to impulse signals or to a white noise process [15]. As discussed in [4], similar definitions arise in the case of LTV systems. We consider the definition based on the average of the response $\mathbf{z}$, when the disturbance input $\mathbf{w}$ is a white-noise process. Suppose that the feedback system of Fig. 4 is well posed, and let $\mathrm{T}_{\mathbf{zw}}$ denote the closed-loop operator from $\mathbf{w}$ to $\mathbf{z}$. Assuming that $\mathbf{x}(0) = 0$, the H_2 performance criterion can be defined as

$$\|T_{\mathbf{zw}}\|_2^2 \triangleq \lim_{n\to\infty} \frac{1}{n} \sum_{k=0}^{n} E[\mathbf{z}(k)^T \mathbf{z}(k)] \tag{19}$$

where $E[.]$ denotes the expectation operator. The discrete-time state feedback H_2 synthesis problem consists of finding (if it exists) a static controller K that stabilizes the closed-loop system and makes the H_2 norm $\|\mathrm{T}_{\mathbf{zw}}\|_2$ of the operator $\mathrm{T}_{\mathbf{zw}}$ smaller than a desired bound $\gamma > 0$. The technique used for controller design relies on results available in [4], [6], and [16], the most important of which are summarized below after being rewritten for the case of affine parameter-dependent systems. In the following, $\mathrm{tr}(L)$, $\mathrm{im}(L)$, and $\ker(L)$ denote the trace, image, and kernel of matrix L, respectively, and A_i, B_i, C_{z_i}, E_i, and B_{w_i} represent the state space matrices of (18) for the $i = 1, \ldots, m$ points in Δ_0.

2) Result 3: A static state feedback controller guarantees quadratic stability of the closed-loop system (18) and ensures that $\|\mathrm{T}_{\mathbf{zw}}\|_2 < \gamma$ for all parameter signals $\boldsymbol{\zeta} : \mathbb{Z}_0^+ \mapsto \mathbb{R}^q$ such that $\boldsymbol{\zeta}(k) \in \Delta$, $k \in \mathbb{Z}_0^+$, if there are real matrices $X = X^T > 0$, K, and Z such that, for $i = 1, \ldots, m$, the following LMI system is satisfied:

$$\begin{bmatrix} X & (A_i + B_i K)X & 0 \\ X(A_i + B_i K)^T & X & X(C_{z_i} + E_i K)^T \\ 0 & (C_{z_i} + E_i K)X & -I \end{bmatrix} > 0 \tag{20}$$

$$\begin{bmatrix} X & B_{w_i} \\ B_{w_i}^T & Z \end{bmatrix} > 0 \tag{21}$$

$$\mathrm{tr}(Z) < \gamma^2. \tag{22}$$

Proof: For the sake of brevity, the proof is only outlined. Since LMIs (20)–(22) are affine functions of $\boldsymbol{\zeta}$, it follows immediately from Result 2 that, if they are satisfied for the $i = 1, \ldots, m$ points in Δ_0, then they are satisfied for all $\boldsymbol{\zeta} \in \Delta$. After some algebraic manipulations, which include applying Schur complements and congruence transformations to (20)–(22), it can be shown that if this system of LMIs is satisfied, then the conditions

$$\begin{cases} A(\boldsymbol{\zeta})^T P A(\boldsymbol{\zeta}) - P + C_z(\boldsymbol{\zeta})^T C_z(\boldsymbol{\zeta}) < 0, \\ \mathrm{tr}(B_w(\boldsymbol{\zeta})^T P B_w(\boldsymbol{\zeta})) < \gamma^2 \end{cases}$$

hold for all $\boldsymbol{\zeta} \in \Delta$ and $P = X^{-1} > 0$. Consequently, the system is quadratically stable and verifies

$$\|T_{\mathbf{zw}}\|_2 < \max_{\boldsymbol{\zeta}\in\Delta} \left(\mathrm{tr}(B_w(\boldsymbol{\zeta})^T P B_w(\boldsymbol{\zeta}))\right)^{1/2} < \gamma.$$

■

The synthesis problem, i.e., that of finding matrices X and Z and controller K that verify (20)–(22), can be solved using the following result.

3) Result 4: Consider the closed-loop system described by (18). If there exist matrices $X = X^T > 0$, M, and Z such that

$$\begin{bmatrix} X & A_iX+B_iM & 0 \\ (A_iX+B_iM)^T & X & (C_{z_i}X+E_iM)^T \\ 0 & C_{z_i}X+E_iM & I \end{bmatrix} > 0 \tag{23}$$

$$\begin{bmatrix} X & B_{w_i} \\ B_{w_i}^T & Z \end{bmatrix} > 0 \tag{24}$$

$$\mathrm{tr}(Z) < \gamma^2 \tag{25}$$

for all $i \in \{1, 2, \ldots, n\}$, then the feedback law $\mathbf{u}(k) = K\mathbf{x}$ with $K = MX^{-1}$ guarantees that the closed-loop system is quadratically stable and $\|\mathrm{T}_{\mathbf{zw}}\|_2 < \gamma$.

Proof: To verify the conditions of Result 3, which ensure quadratic stability and the γ upper-bound on $\|\mathrm{T}_{\mathbf{zw}}\|_2$, the matrices $X = X^T > 0$, K, and Z must satisfy (20)–(22). Applying the simple change of variables $M = KX$ to (20), we obtain (23), thus showing that the conditions are met. ■

Note that the change of variables $M = KX$ transforms the synthesis problem into an LMI feasibility test on X, M, and Z and that the matrix gain K can be simply obtained from $K = MX^{-1}$. Finally, the optimal solution for the H_2 control synthesis problem is approximated through the minimization of γ subject to the conditions specified in Result 4.

B. Preview Controller Synthesis Technique

For augmented discrete-time dynamic systems that include large preview intervals $p > 50$, the controller synthesis technique proposed in the last section leads to LMI optimization problems involving a large number of variables, which cannot easily be solved using the tools available today.

Going back to the preview control problem, consider the linear discrete-time system (17). It is well known from the literature [1], [2], [10] that solutions to H_2 discrete-time preview control problems can, in general, be decomposed into feedback and feedforward controllers by exploiting the particular structure of the augmented preview dynamics. Building on these ideas, an alternative algorithm for computing the feedforward gain matrix is presented.

To start with, consider an affine parameter-dependent system with the structure of (17), defined over a region Δ, with its m vertices in Δ_0. Restricting the dependence on the parameter to the state equation, let $\bar{A}_i$, $\bar{B}_i$, $\bar{B}_{w_i}$, $\bar{C}_z$, and $\bar{E}$ denote the state space matrices for the $i = 1, \ldots, m$ points in Δ_0. Assuming that $\mathbf{s}$ belongs to the disturbance vector $\mathbf{w}$, matrix $\bar{B}_{w_i}$ includes the preview input matrix $\bar{B}_s$. Consider also the central point of Δ, $\boldsymbol{\zeta}_o$, and the corresponding state space matrices $\bar{A}_o$, $\bar{B}_o$, and $\bar{B}_{w_o}$.

Partitioning matrices according to the augmented system structure, let $P = \begin{bmatrix} P_d & P_{ds} \\ P_{ds}^T & P_s \end{bmatrix}$, $Q = \bar{C}_z^T\bar{C}_z = \begin{bmatrix} Q_d & Q_{ds} \\ Q_{ds}^T & Q_s \end{bmatrix}$, $R = \bar{E}^T\bar{E}$, and $K = [K_d\ ,\ K_s]$. Instead of computing K_d and K_s simultaneously for the augmented system (17), we propose a design methodology that comprises the following steps: 1) design a state-feedback H_2 controller for the original affine parameter-dependent system without preview and 2) given the resulting feedback gain matrix K_d, compute the feedforward gain matrix K_s to meet specific performance criteria for the system evaluated at the central point of Δ.

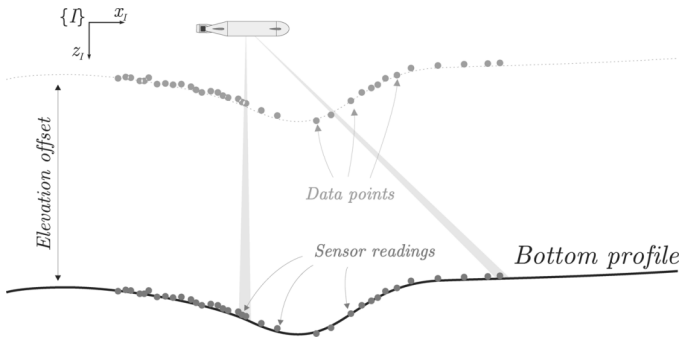

Fig. 5. Sensor readings and elevation offset to obtain the data points used in the algorithm.

The following result provides a procedure to compute an alternative feedforward controller $\mathrm{K}_{\mathbf{s}}$ with a feasible computation time; see [10] for further details.

Theorem 1: Given a pair (P_d, K_d), $P_d = P_d^T > 0$ that satisfies the conditions of Result 3, consider the matrix

$$P_{ds} = [\tilde{A}_c^T P_d B_o, (\tilde{A}_c^2)^T P_d B_o, \ldots, (\tilde{A}_c^{p+1})^T P_d B_o] + [Q_1, \tilde{A}_c^T Q_1 + Q_2, \ldots, \sum_{j=1}^{p+1} (\tilde{A}_c^{p+1-j})^T Q_j]$$

where $\tilde{A}_c = A_o - B_o\left(B_o^T P_d B_o + R\right)^{-1} B_o^T P_d A_o$ and Q_j denotes the jth s-dimensional column block of matrix Q_{ds}. Consider also the feedforward gain matrix

$$K_s = \left(B_o^T P_d B_o + R\right)^{-1} B_o^T \left(P_d H_o + P_{ds} D\right). \tag{26}$$

Then, the resulting closed-loop system (18) is stable over the whole region Δ and the Lyapunov inequality for the central point verifies

$$(\bar{A}_o+\bar{B}_oK)^T P(\bar{A}_o+\bar{B}_oK) - P + (\bar{C}_z+\bar{E}K)^T(\bar{C}_z+\bar{E}K) \leq 0$$

with $P = P^T > 0$.

VI. Reference Path

The preview-based tracking controller presented in the previous sections can be applied to bottom-following for AUVs using different range-sensing techniques. In this paper, a setup is considered wherein two narrow beam echo sounders, mounted underneath the vehicle, scan the seabed along the vehicle's direction of forward motion; see Fig. 5. As a result of this setup, a vector of reference points expressed in the inertial coordinate system is available, and the full preview vector $\mathbf{x}_s(k)$ can be computed at every sampling instant.

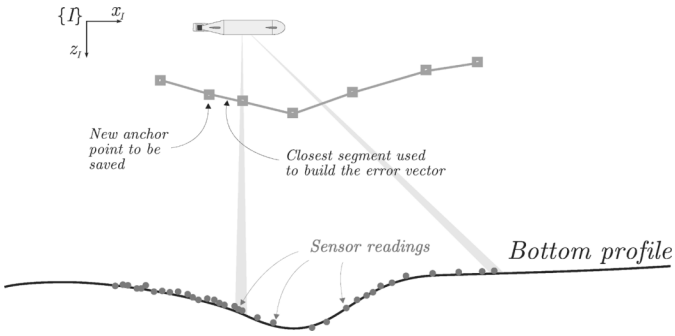

Fig. 6. Final computed path composed by segments of straight lines.

The method adopted to build the reference path from measurement data is now briefly introduced. The output of the echo sounders expressed in the inertial frame $\{I\}$ is saved in a vector sorted by increasing values of the x coordinate, after adding in the elevation offset (defined as the offset that the vehicle should keep above the seabed). See Fig. 5. These points are then converted into a path composed by the concatenation of a set of straight lines according to the following algorithm. At each sampling time, the algorithm starts by considering an anchor point that corresponds to the last way point visited by the vehicle; this will be the starting point of the current algorithm iteration. Afterwards, the algorithm creates a series of way points equidistant by approximately $N_w V_t T$, each one corresponding to the centroid of data points located inside a ball of radius $N_w V_t T$. The way points are then interpolated by straight lines to approximate the seabed profile. Fig. 6 presents the result of applying the proposed path reconstruction technique to the data points displayed in Fig. 5. Using centroids to compute the way points avoids sudden changes in the reference path between sampling instants when new data points are added. Furthermore, this simple reference building technique has a relatively high immunity to sonar sensor noise. If a large number of data points are available, the centroids provide some inertia to the inclusion of new data points, and, for reasonable values of N_w, the way points are always located over or very near a cloud of data points.

VII. Implementation

The design and performance evaluation of the overall closed-loop system was done using the model described in Section II.

A. Affine Parameter-Dependent Description of the Plant

In the application presented here, the vehicle is expected to follow a reference path, in the vertical plane, composed by the concatenation of straight lines. During the controller design phase, the considered AUV's flight envelope was parameterized by $\boldsymbol{\zeta} = [V_r, \gamma_T]^T$ (equivalently by $[u, w]^T$) and partitioned in the 19 regions presented in Fig. 7. For each operating region, the elements of the discrete-time state space matrices were obtained from the linearization of the error dynamics over a dense grid of operating points and then approximated by affine functions of $\boldsymbol{\zeta}$ using a least squares fitting. As an example, Fig. 8 shows the surface obtained for element (2,3) of matrix $\bar{A}$ and the planes computed for the considered set of operating regions. For a relatively dense grid of evaluated operating points, the affine approximation results in a maximum absolute error between entries of the matrices of less than 3% and an average absolute error of less than 1.4%.

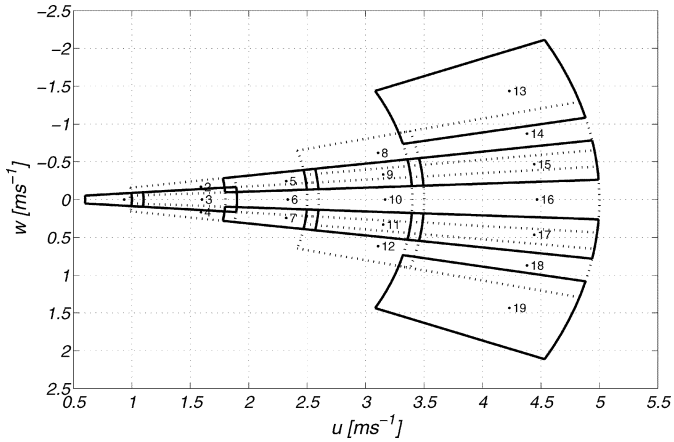

Fig. 7. Operating regions parameterized by $\boldsymbol{\zeta}$ and plotted in the body velocity axes.

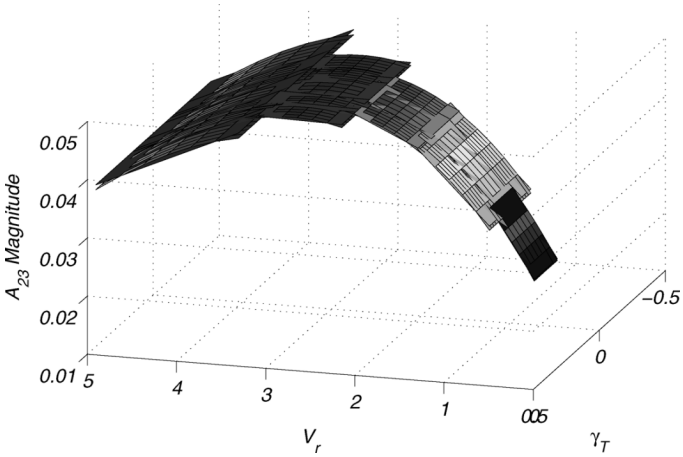

Fig. 8. Surface and respective affine approximation obtained for element A_{23} as a function of the velocity V_r and angle of attack γ_T.

B. Controller Implementation

To implement the controller under the scope of gain scheduling control theory, a state feedback matrix gain $\mathrm{K}_i = [\mathrm{K}_{di}, \mathrm{K}_{si}]$, $i = 1, \ldots, 19$, was computed for each of the operating regions using the technique presented in Section V. During the controller design phase, the regions were defined overlapped to avoid fast switching between controllers, see Fig. 7. The disturbance input matrix $\bar{B}_w$ was set to $\bar{B}_s$ and the state and control weight matrices $\bar{C}_1$ and $\bar{D}_{12}$, respectively, were set to yield the performance vector $\mathbf{z}(k) = [\mathbf{z}_1(k)^T\ \mathbf{z}_2(k)^T\ \mathbf{z}_3(k)^T]^T$, where

$$\mathbf{z}_1 = \Big[\sqrt{20}\,u_e, \sqrt{8}\,w_e, \sqrt{0.1}\,q_e, \sqrt{30}\,d_T, \theta_e, x_{i1}, \quad (27)$$

$$\sqrt{0.1}\,x_{i2}, \sqrt{10}\,x_{i3}\Big]^T \quad (28)$$

$$\mathbf{z}_2 = [W_1(z)\,\delta_b, W_2(z)\,\delta_c]^T \quad (29)$$

$$\mathbf{z}_3 = \Big[\sqrt{5}\,\delta_b, \sqrt{5}\,\delta_c, \sqrt{0.1}\,T_C\Big]^T \quad (30)$$

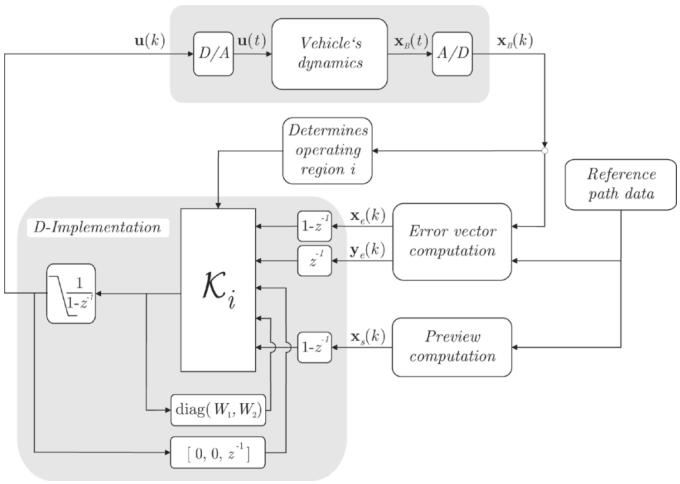

Fig. 9. Implementation setup using gain scheduling and the D-methodology.

and $W_j(z)$, $j = 1, 2$, are second-order high-pass filters implemented by the strictly proper transfer function $W_j(z) = 90(z-0.999)/(z-1)(z-0.9)$ that weights the bow and stern control surface signals with the objective of limiting the corresponding actuator bandwidths. Furthermore, the third integral state x_{i3} corresponds to discrete time integral action on the bow control surface δ_b which introduces a "washout" to ensure zero bow plane deflection at trimming, see [13].

The final implementation scheme, presented in Fig. 9, was achieved using the D-methodology described in [11]. This methodology moves all integrators to the plant input and adds differentiators where they are needed to preserve the transfer functions and the stability characteristics of the closed-loop system. The resulting gain scheduled control law exhibits two main properties:

- *Linearization property*: The linearization of the nonlinear gain scheduled feedback control system about each trimming trajectory preserves the internal as well as the input-output properties of the corresponding linear closed loop designs.
- *Auto trimming property*: The nonlinear controller implementation does not require that the trimming values of all state variables and inputs be fed into the controller.

The methodology is based on the key observation that, in a gain scheduling setting, linear controllers are designed to operate on perturbations of the plant's inputs and outputs about equilibrium points. This is achieved by differentiating some of the measured outputs before they are fed back to the gain scheduled controller. In order to preserve the input–output behavior of the feedback system, integral action is provided at the input to the plant. The integrators hold the key to the success of the methodology, as they naturally "charge up" to the input values required to trim the plant.

Fig. 10 presents the entries of the preview feedforward control matrix $\mathrm{K_s}$ as a function of the preview time, for all of the operating regions. In this case, a preview interval of 20 s, sampled at $T = 0.1$ s, is considered. From the figure, it becomes clear that the weight of the preview signal decreases as the corresponding instant of time is further ahead in the future, with negligible contributions above 15 s of preview time. The width of the preview interval suitable for a given vehicle is a compromise between the time constants associated with the vehicle's dynamics, the computational power available onboard, and the actual sonar range. In the present case, for a maximum vehicle speed of 2.5 m/s and assuming a sonar range of 50 m provided by a 600-kHz pencil beam sonar, it will be reasonable to consider a preview interval of 15 s, which corresponds to a preview length of 150 samples. An additional analysis tool, which is used to assess the performance of the preview control scheme, consists of comparing the H_2 norm of the linear closed-loop systems resulting from applying the control strategies with and without preview action. As shown in Fig. 11, considering a mesh of operating points defined by the parameter vector $\boldsymbol{\zeta}$, the performance index for the preview H_2 feedback–feedforward compensator is consistently below the classical H_2 feedback solution obtained for the same performance index.

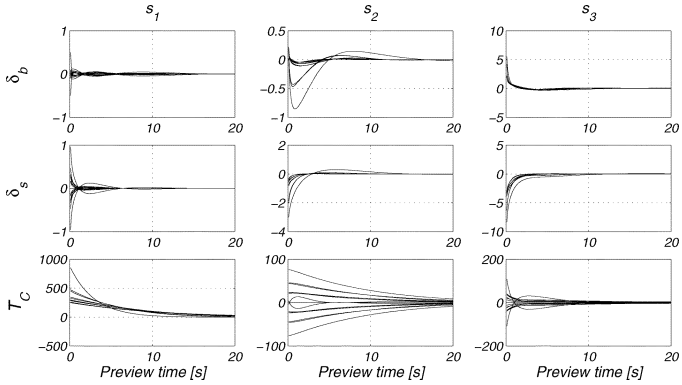

Fig. 10. Evolution of the preview gains as a function of preview time.

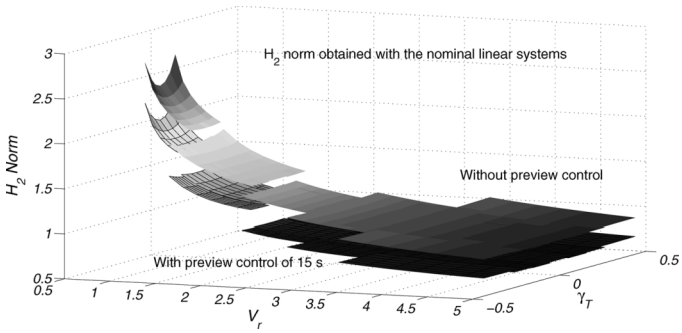

Fig. 11. Closed-loop system's H_2 norm obtained with and without preview.

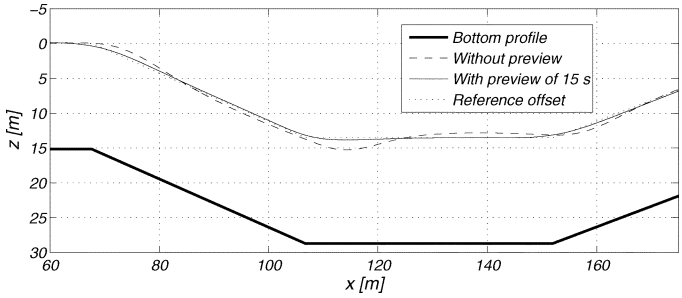

Fig. 12. Trajectories described by the vehicle, with and without preview.

VIII. Simulation Results

Here, an artificial seabed profile with very sharp transitions is used to evaluate the performance of the bottom-following

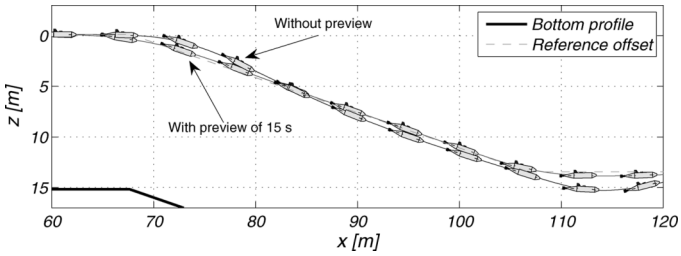

Fig. 13. Detail of the trajectories described by the vehicle: Descending phase. Fig. 12 for $t \in [60, 120]$ s.

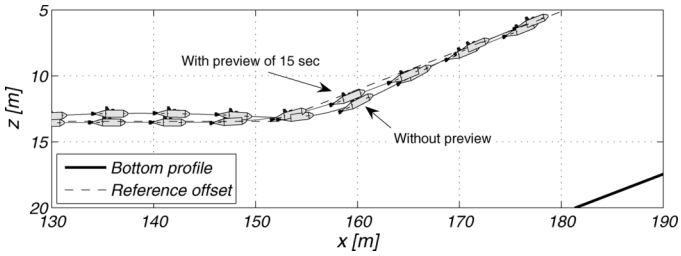

Fig. 14. Detail of the trajectories described by the vehicle: Climbing phase. Fig. 12 for $t \in [130, 190]$ s.

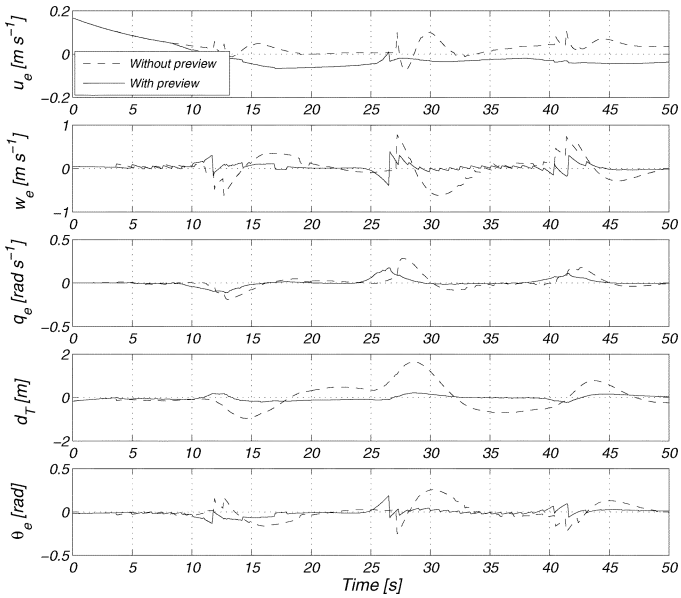

Fig. 15. Time evolution of the error vector $\mathbf{x}_e(t)$, with and without preview.

techniques. The control objective is to achieve a constant 15-m bottom elevation offset. Fig. 12 shows that, for constant slopes, the vehicle trajectory converges to the designated elevation offset. It also shows that the inclusion of preview control action results in a smoother path trajectory, largely reducing overshoots and the convergence time.

A detailed view of the trajectory described by the vehicle is displayed in Figs. 13 and 14, which include three seabed's slope transitions of the maneuver. The figures show clearly that the use of preview yields better tracking performance.

The time evolution of the error state vector $\mathbf{x}_e$ without preview and with a preview of 15 s is presented in Fig. 15. It can be observed that, due to the preview action, the signal activity clearly precedes the path transition points. The actuation signals

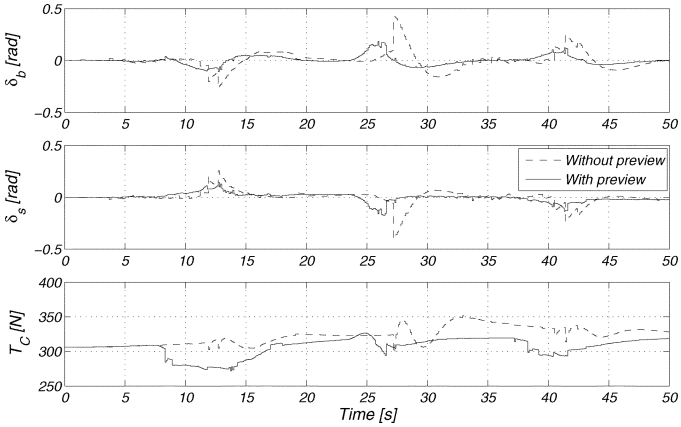

Fig. 16. Time evolution of the actuation $\mathbf{u}(t)$ with and without preview.

for the same experiments can be compared in Fig. 16, and it is also clear that, with preview, the excursion of the resulting actuation signals is significantly reduced, and both the state and input variables converge to the trimming conditions faster. The actuation signals also reflect the unavoidable problem of additional disturbances introduced by the sonar data acquisition and processing, which are nevertheless greatly reduced by the dynamic weights introduced to limit the closed loop actuator bandwidths.

IX. Conclusion

This paper presented the design and performance evaluation of a bottom-following controller for AUVs.

Resorting to an H_2 controller design methodology for affine parameter-dependent systems, the technique presented exploited an error vector that naturally describes the particular dynamic characteristics of the AUV for a suitable flight envelope.

An algorithm was used for the computation of the feedforward gain matrix that avoids solving LMIs involving a large number of unknowns. The resulting nonlinear controller was synthesized and implemented under the scope of gain-scheduling control theory, using a piecewise affine parameter-dependent model representation, for the given set of operating regions.

The effectiveness of the new control laws was assessed in the MATLAB/Simulink simulation environment with a vertical plane nonlinear dynamic model of the INFANTE AUV. The quality of the results obtained clearly indicate that the methodology derived reduces the path following error and simultaneously smooths the actuation signal.

References

[1] M. Tomizuka, "Optimum linear preview control with application to vehicle suspension-revisited," *ASME J. Dynam. Syst., Meas., Control*, vol. 98, no. 3, pp. 309–315, 1976.

[2] G. Prokop and R. S. Sharp, "Performance enhancement of limited bandwith active automotive suspensions by road preview," *Proc. IEE Control Theory Appl.*, vol. 142, no. 2, pp. 140–148, 1995.

[3] K. Takaba, "Robust servomechanism with preview action for polytopic uncertain systems," *Int. J. Robust Nonlinear Control*, vol. 10, pp. 101–111, 2000.

[4] , L. E. Ghaoui and S. I. Niculescu, Eds., *Advances in Linear Matrix Inequality Methods in Control*. Philadelphia, PA: SIAM, 1999.

[5] S. Boyd, L. E. Ghaoui, E. Feron, and V. Balakrishnan, *Linear Matrix Inequalities in Systems and Control Theory*. Philadelphia, PA: SIAM, 1994.
[6] P. Gahinet, P. Apkarian, and M. Chilali, "Affine parameter-dependent Lyapunov functions and real parametricuncertainty," *IEEE Trans. Autom. Control*, vol. 41, no. 3, pp. 436–442, Jun. 1996.
[7] R. Cunha and C. Silvestre, "A 3-D path-following velocity-tracking controller for autonomous vehicles," in *Proc. 16th IFAC World Congress*, Praha, Czech Republic, Jul. 2005, vol. 16, pp. 73–79.
[8] C. Silvestre, A. Pascoal, and I. Kaminer, "On the design of gain-scheduled trajectory tracking controllers," *Int. J. Robust Nonlinear Control*, vol. 12, pp. 797–839, 2002.
[9] I. Kaminer, A. Pascoal, E. Hallberg, and C. Silvestre, "Trajectory tracking for autonomous vehicles: An integrated approach to guidance and control," *AIAA J. Guid., Control, Dynam.*, vol. 21, no. 1, pp. 29–38, 1998.
[10] N. Paulino, C. Silvestre, and R. Cunha, "Affine parameter-dependent preview control for rotorcraft terrain following flight," *J. Guid., Control, Dynam.*, vol. 29, no. 6, 2006.
[11] I. Kaminer, A. Pascoal, P. Khargonekar, and E. Coleman, "A velocity algorithm for the implementation of gain-scheduled controllers," *Automatica*, vol. 31, no. 8, pp. 1185–1191, 1995.
[12] C. Silvestre, "Multi-objective optimization theory with applications to the integrated design of controllers/plants for autonomous vehicles," Ph.D. dissertation, Dept. of Elect. Eng., Instituto Superior Técnico, Lisbon, Portugal, 2000.
[13] C. Silvestre and A. Pascoal, "Depth control of the infante auv using gain-scheduled reduced order output feedback," *Control Eng. Practice*, vol. 15, no. 7, pp. 883–895, 2007.
[14] T. Fossen, *Guidance and Control of Ocean Vehicles*. New York: Wiley, 1994.
[15] K. Zhou, J. C. Doyle, and K. Glover, *Robust and Optimal Control*. Upper Saddle River, NJ: Prentice-Hall, 1995.
[16] C. Scherer and S. Weiland, *Lecture Notes on Linear Matrix Inequalities in Control*. Delft, The Netherlands: Dutch Inst. of Systems and Control, 2000.

Carlos Silvestre received the Licenciatura and M.Sc. degrees in electrical engineering and the Ph.D. degree in control science from the Instituto Superior Técnico (IST), Lisbon, Portugal, in 1987, 1991, and 2000, respectively.

Since 2000, he has been with the Department of Electrical Engineering, IST, where he is currently an Assistant Professor of Control and Embedded Architectures for Real Time Control Applications. Over the past years, he has been conducting research at the Institute for Systems and Robotics on the subjects of vehicle and mission control of air and underwater robots. His research interests include linear and nonlinear control theory, coordinated control of multiple vehicles, gain scheduled control, integrated design of guidance and control systems, inertial navigation systems, and mission control and real-time embedded architectures for complex autonomous systems with applications to unmanned air and underwater vehicles.

Rita Cunha received the Licenciatura degree in information systems and computer engineering and the M.Sc. and Ph.D. degrees in electrical and computer engineering from the Instituto Superior Técnico (IST), Lisbon, Portugal, in 1998, 2002, and 2007, respectively.

She is currently a Postdoctoral Researcher with the Institute for Systems and Robotics, IST. Her research interests include guidance and control of autonomous vehicles, rigid body stabilization, sensor-based control, and modeling of small-scale helicopters and quadrotors.

Nuno Paulino received the Licentiate's degree in electrical engineering and the M.Sc. degree in decision systems and control from the Instituto Superior Técnico (IST), Lisbon, Portugal, in 2002 and 2005, respectively.

He worked on research at the Institute for Systems and Robotics, IST, on the subjects of vehicle control of air and underwater robots until 2006. During 2006–2008, he enrolled in a traineeship program at ESTEC/ESA facilities in The Netherlands, integrated in the Control Systems Division. Recent work concerns spacecraft attitude and orbit control systems, robust control law algorithm analysis and design, fault isolation, and reconfiguration control in space applications.

António M. Pascoal received the Ph.D. degree in control science from the University of Minnesota, Minneapolis, in 1987.

He is currently an Associate Professor with the Instituto Superior Técnico (IST), Lisbon, Portugal. In 1993 he joined the Institute for Systems and Robotics (ISR) of IST, where he is the Coordinator of the Dynamical Systems and Ocean Robotics Laboratory. Over the past several years, he has participated actively in the design, development, and operation of prototype marine robots, including autonomous surface craft and underwater vehicles. He has coordinated several European projects aimed at bridging the gap between marine science and technology. His research interests include linear and nonlinear control theory, integrated design of navigation, guidance and control systems, and cooperative motion control of multiple vehicles under severe communication constraints. He is also interested in the history of science, animal navigation and locomotion, and the application of marine robotics to underwater archaeology.